

A study of major mergers using a multi-phase ISM code

J. Weniger^{1,*}, Ch. Theis¹, and S. Harfst²

¹ Institut für Astronomie, Universität Wien, Türkenschanzstraße 17, 1180 Wien, Austria

² Leiden Observatory, Leiden University, PO Box 9513, 2300 RA Leiden, the Netherlands

The dates of receipt and acceptance should be inserted later

Key words galaxies: interactions, galaxies: spiral, galaxies: ISM, ISM: clouds, stars: formation

Galaxy interactions are a common phenomenon in clusters of galaxies. Especially major mergers are of particular importance, because they can change the morphological type of galaxies. They have an impact on the mass function of galaxies and they trigger star formation - the main driver of the Galactic Matter Cycle. Therefore, we conducted a study of major mergers by means of a multi-phase ISM code. This code is based on a TREE-SPH-code combined with a sticky particle method allowing for star formation controlled by the properties of a multi-phase ISM. This is in contrast to the usually implemented Schmidt law depending mainly on the gas density. Previously, this code was used on isolated galaxies. Since our star formation recipe is not restricted to a special type of galaxy, it is interesting to apply it to interacting galaxies, too. Our study on major mergers includes a research of global properties of the interacting system, namely the star formation rate and the star formation efficiency, the evaporation and condensation rates, as well as the mass exchange of distinct components, namely stars, diffuse ISM, and clouds. Investigating these properties provides insight to interrelations between various physical processes. The results indicate that the star formation efficiency as well as the evaporation and condensation rates are influenced by the interaction.

© 2009 WILEY-VCH Verlag GmbH & Co. KGaA, Weinheim

1 Introduction

For some decades it has been known, that galaxy interactions play an important role in the evolution of galaxies changing their morphological type or triggering star formation. Since it is possible to take remarkable pictures of peculiar galaxies (see e. g. Arp 1966), the question was raised if their features are a result of galaxy interactions. Peculiar features are e.g. bridges connecting galaxies or tails protruding from them. The above mentioned assumption seemed likely, however, it was not clear until numerical simulations corroborated it. The first simulations only considered gravitational forces (e.g. Holmberg 1941; Pleiderer & Siedentopf 1961; Toomre & Toomre 1972; Barnes 1988), using different simplifications on the force calculation owing to the limited computing power at that time. Nevertheless, those simulations already demonstrated, that interactions between galaxies change their appearance.

Simulations became more sophisticated with increasing computer power. Hence, it was feasible to address topics concerning the interstellar medium (ISM). Though the ISM only contributes approximately 10% of the mass of present-day galaxies, it is still an important ingredient: firstly, all stars are formed within the cold phase of the ISM, the molecular clouds. Hence, it is necessary to consider this component in order to study the star formation rate during galaxy interactions. Secondly, the dynamics are strongly influenced by hydrodynamics and especially energy dissipation. Which properties of the ISM are considered depends

on the code used (see e.g. the review by Barnes & Hernquist 1992). Our code incorporates a 3-phase ISM similar to the proposition by McKee & Ostriker (1977). The code was developed in order to study Milky Way-like galaxies accounting for several components, namely stars, dark matter, and the three phases of the ISM (Harfst et al. 2006). The warm and hot phases are treated by smoothed particle hydrodynamics implemented similar to Hernquist & Katz (1989). The molecular clouds are modelled by the sticky particle method (for details refer to Theis & Hensler 1993). A similar code was used by Semelin & Combes (2002), but they used a different sticky particle method and a different star formation prescription.

Major mergers, that are interacting galaxies of about equal size, are studied by numerous authors. Often the research's aim is to study the properties of the remnant galaxy (e.g. Barnes 1988; Springel & Hernquist 2005), or to look for substructures, such as tidal dwarf galaxies (Duc et al. 2004; Bournaud & Duc 2006; Wetzstein et al. 2007). Other goals are the reproduction of observed major mergers (e.g. Karl et al. 2008), or to study the overall properties of interacting galaxies, such as the star formation rate (e.g. Mihos & Hernquist 1996; di Matteo et al. 2008). While studying the star formation most often the Schmidt-Kennicutt relation (Schmidt 1959; Kennicutt 1998) or some modification of it are used. The Schmidt-Kennicutt relation says that the star formation rate is proportional to the gas density, with the proportionality factor being a constant star formation efficiency. This work is distinct in that respect, since it does not use the Schmidt-Kennicutt relation, but uses a star formation prescription following Elmegreen & Efremov (1997).

* e-mail: julia.weniger@univie.ac.at

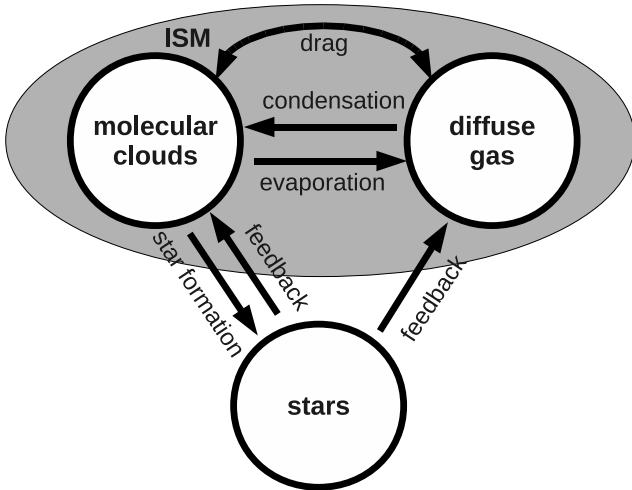


Fig. 1 A scheme of all physical processes connecting the different components of a galaxy. In addition, the gas loses energy by radiative cooling and the molecular clouds by inelastic collisions.

They found that the star formation efficiency is not fixed, but dependent on local properties of the ISM, i.e. the mass of the star forming cloud and the pressure in the ambient ISM.

The main aim of this work is to study the evolution of the star formation during a major merger. In particular we are interested in understanding how a locally defined star formation efficiency affects the star formation rate. Our study also yields the mass exchange rates due to condensation and evaporation.

2 Interactions between different components

The interaction participants are described by particles mimicking distinct components of a galaxy, namely stars, diffuse gas, molecular clouds, and dark matter particles. Those components are connected by various physical processes (see Fig. 1). The processes condensation, evaporation, and a drag force due to ram pressure allow for matter and momentum exchange between the diffuse ISM and the clumpy molecular clouds. Star formation and related feedback of supernovae type II and planetary nebulae close the circuit of matter. Energy dissipation is caused by radiative cooling in case of the diffuse ISM and by inelastic collisions in case of molecular clouds. Since studying the evolution of star formation is the main aim of this work, the next section will describe its implementation in more detail. For a thorough description of all other processes we refer to Harfst et al. (2006).

2.1 Star formation

The site of star formation is known to be giant molecular clouds (e.g. Lada & Lada 2003). Since they are represented in our code by sticky particles, those particles have to be

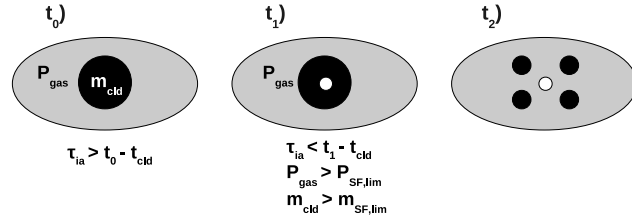


Fig. 2 The star formation scheme according to Harfst et al. (2006). First the molecular cloud is inactive for a period τ_{ia} (t_0). After that time span, a "star cluster" is formed within the molecular cloud provided that all other star formation criteria are fulfilled (t_1). The mass of the embedded star cluster is dependent on the local star formation efficiency, ϵ . Finally, the cloud is fragmented due to energy input from supernovae type II and the ambient gas is heated (t_2).

converted to star particles. The implementation of it works as follows (Fig. 2):

- We assume that it takes $\tau_{ia} = 200 \text{ Myr}$ till gas in a molecular cloud is able to form stars. During this time the molecular cloud is inactive. In other words, star formation is suppressed as long as the age of the molecular cloud, $t_{\text{now}} - t_{\text{cld}}$ is smaller than τ_{ia} . τ_{ia} is the only free parameter in our star formation prescription and can be interpreted as a global star formation time scale. It is gauged by the star formation rate of the Milky Way. Since the mean star formation efficiency, ϵ , in our simulations is approximately 5% (see Fig. 4) and the total mass in molecular clouds is approximately $4 \cdot 10^{11} M_{\odot}$ (see Table 1), it gives a mean star formation rate of approximately $\text{SFR} = \tau_{ia}^{-1} \cdot \epsilon \cdot M_{\text{cld}} \approx 1 M_{\odot} \text{ yr}^{-1}$.
- Afterwards stars can be formed. They stay embedded in their parent molecular cloud. Their mass is determined by the star formation efficiency, ϵ . A mass criterion and a pressure criterion prevent the formation of too small stellar particles: the mass of the molecular clouds, m_{cld} , must exceed $2.5 \cdot 10^4 M_{\odot}$ and the pressure at the position of the molecular cloud, P_{gas} , must be higher than a tenth of the ISM pressure at the position of the Sun in the Milky Way, i.e. $P_{\odot} = 3 \cdot 10^4 \text{ K cm}^{-3}$ (Elmegreen & Efremov 1997). Note, that the star formation efficiency is not constant, but it depends on local properties, namely the gas pressure and the mass of the parent molecular cloud.
- After the most massive stars end their lives as supernovae, the molecular cloud fragments into four pieces of equal mass due to feedback by supernovae.

3 Numerical setup

Following Harfst et al. (2006) the initial galaxies were constructed by firstly generating a disk/bulge/halo - system using the method of Kuijken & Dubinski (1995). In the next step, one fifth of the stellar disk particles were transformed into molecular clouds and finally the diffuse ISM was added as an initially slowly rotating homogeneous sphere, which

Table 1 Mass of distinct components of one galaxy and corresponding number of particles

Component	Mass [$10^{11}M_{\odot}$]	NR. of particles
Bulge-stars	0.17	10000
Disk-stars	0.29	75098
Clouds	0.04	36347
Gas-particles	0.02	9017
DM-particles	1.94	100000
Total	2.46	230462

will collapse in the first 200 Myr forming a warm disk. The collisionless model of Kuijken & Dubinski (1995) realises an equilibrium configuration. However, the equilibrium is affected by adding the ISM and the above mentioned processes. Therefore, we follow the system's evolution, until a quasi-equilibrium is established. The numerical integration is done by means of a TREE-SPH code combined with the sticky particle method (Theis & Hensler 1993). Gravitational forces are determined by the DEHNEN-Tree (Dehnen 2002). See Harfst et al. (2006) for a more thorough description.

The relaxed galaxy has a mass of $2.46 \cdot 10^{11} M_{\odot}$, thereof 79% in dark matter particles. The remaining baryonic matter consists of approximately 12% ISM particles - hence, molecular clouds and diffuse ISM - the rest being disk and bulge stars. The galaxy is realised by a total number of 230462 particles. Note, that not only the mass, but also the number of clouds, SPH-particles, and disk stars as given in Table 1 will change throughout the simulations: this is caused by inelastic collisions, star formation, and feedback. The numbers of dark matter particles (10^5) and bulge stars (10^4), on the other hand, stay constant throughout the simulations. Both galaxies are of equal mass and their rotation is prograde. The galactic planes coincide with the orbital plane. At $t = 0$ the galaxies are placed at a separation of 100 kpc. Their initial speed is chosen to match a parabolic orbit with a minimum separation of 20 kpc. The run was stopped at $t = 3$ Gyr.

4 Results

The code configuration allows to follow the evolution of different components and their interrelations. To illustrate the time evolution, a series of snapshots are plotted in Fig. 3 exhibiting the surface density of the cold phase. The distribution of the cold phase resembles the distribution of the stars very well. This implies that dissipation does not affect the cold phase severely. In contrast, the diffuse ISM shows a slightly different distribution (see also Fig. 7). The first snapshot of Fig. 3 (top, left) shows the initial configuration. The first passage at $t = 400$ Myr is pictured in the second panel (top, middle). Afterwards, a series of snapshots features on the one hand the expansion of the tails and on the other hand the development of a bridge, which vanishes gradually. The bottom row of Fig. 3 shows a snapshot shortly before the

second passage which takes place at $t = 1520$ Myr, the beginning of the merging at $t = 1650$ Myr, and a quiescent phase after the merging ($t = 2000$ Myr). The beginning of the merging is defined by the last local minimum in the potential energy of the system, after which the centre of mass of the bulge components are no longer separating. In addition, Fig. 4 shows the star formation rate, the star formation efficiency, the number of star formation processes per 10 Myr, the evaporation and condensation rate and the evolution of the masses of the different components. The vertical dashed lines in Fig. 4 indicate the first encounter, the second encounter, and the beginning of the merging.

The star formation rate shows fluctuations due to the limited number of star formation processes during measurement intervals of 10 Myr. Still it is obvious that there is a maximum in the star formation rate at 1690 Myr, shortly after the merging starts. Another local maximum is given at 610 Myr, that is 210 Myr after the first passage. However, Fig. 4 suggests an enhanced star formation already prior to the first passage. The period of enhanced star formation located around the first passage is more than 400 Myr long. In this setup, the reason for enhanced star formation is not an enhanced number of star formation processes, but an enhanced star formation efficiency: the number of star formation processes does not correlate well with the star formation rate, but the star formation efficiency does, as one can easily infer from the left side of Fig. 4. Only the enhanced star formation prior to the first encounter cannot be explained by an enhanced star formation efficiency. Here, it seems that the number of star formation processes is crucial. Although the mean star formation efficiency is only 5%, the maximum star formation efficiency found within a time step can even exceed 50%. In general, Fig. 6 suggests, that the merging facilitates higher star formation efficiencies. In fact, the maximum star formation efficiency is in the mean about 9% higher after $t = 1650$ Myr. Fig. 5 features a map of the star formation efficiency at $t = 550$ Myr, hence 150 Myr after the first passage. The star formation efficiency is highest in the centre of the galaxies, but also sites of enhanced star formation efficiency are recognised in the bridge and the tails. Though the star formation rate is affected by the interaction, it is still not extraordinary high. Previous research (e.g. Cox et al. 2004) implies that the magnitude of the star formation rate depends on the initial conditions, especially on the orbit. Furthermore the fraction of mass in molecular clouds might be too low to obtain a starburst of several tens up to several hundreds $M_{\odot} \text{ yr}^{-1}$.

Other important quantities are the evaporation and condensation rates. The local maxima in the evaporation rate (at $t = 630$ Myr and at $t = 1710$ Myr) take place approximately 20 Myr after the local maxima in the star formation rate. This time interval corresponds to the time delay between star formation and feedback due to energy input of supernovae. Note, however, that the time resolution is only 10 Myr. The condensation rate has its maximum at exactly the same time the merging starts. During this episode

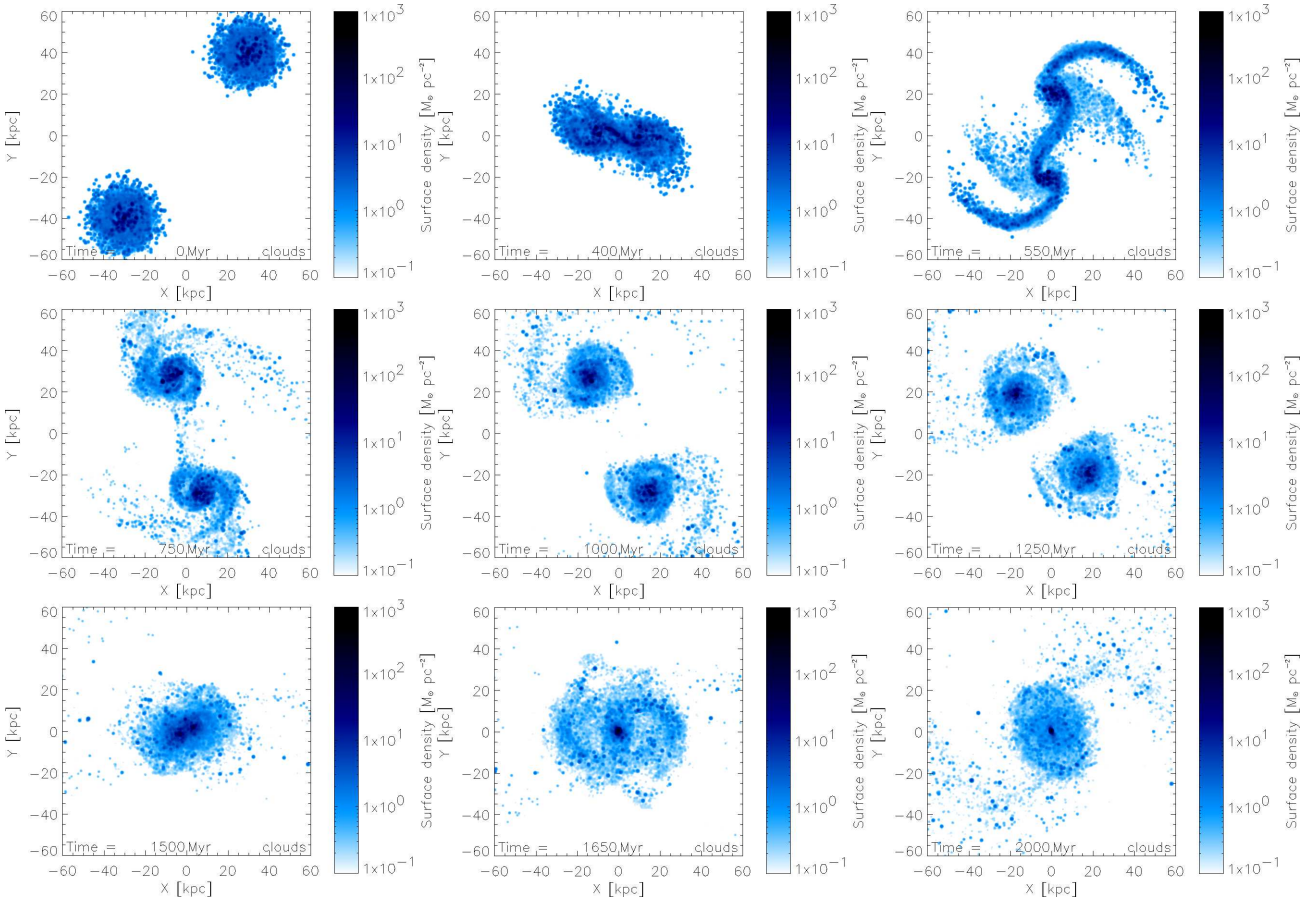


Fig. 3 Snapshots of the interaction. Surface density maps of the clouds are shown (from left to right and top to bottom: t equals 0, 400, 550, 750, 1000, 1250, 1500, 1650, 2000 Myr). The first passage takes place at $t = 400$ Myr, the second at $t = 1520$ Myr, and the merging starts at $t = 1650$ Myr.

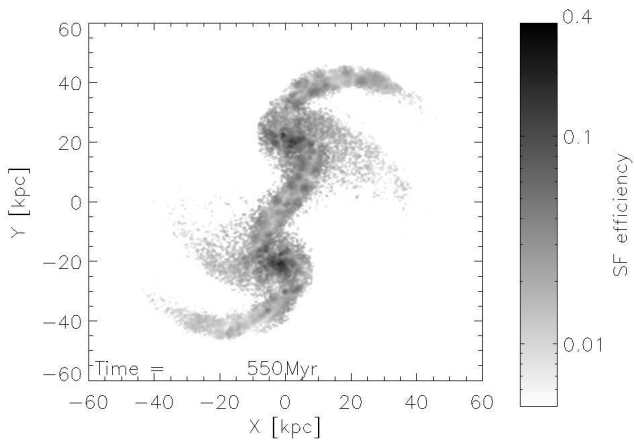


Fig. 5 The star formation efficiency at $t = 550$ Myr.

condensation outweighs evaporation. In general, however, evaporation exceeds condensation. The mean value for the former is $1 M_{\odot} \text{ yr}^{-1}$ and for the latter $0.8 M_{\odot} \text{ yr}^{-1}$. A high condensation rate coinciding with the beginning of the merging, has also been found in other major mergers performed by us so far. The understanding of this remarkable feature and its implications will be the topic of further study.

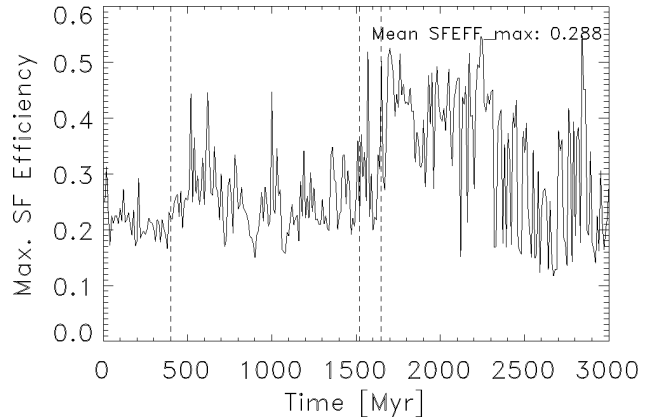


Fig. 6 Evolution of the maximum star formation efficiency. The three vertical dashed lines indicate the first passage, the second passage, and the beginning of the merging.

Altogether the mass evolution of distinct components shows the following features (see middle and bottom diagram of Fig. 4)

- In general, the cloud mass is depleted by star formation while the stellar mass increases continuously. Furthermore, the cloud mass decreases, because evaporation

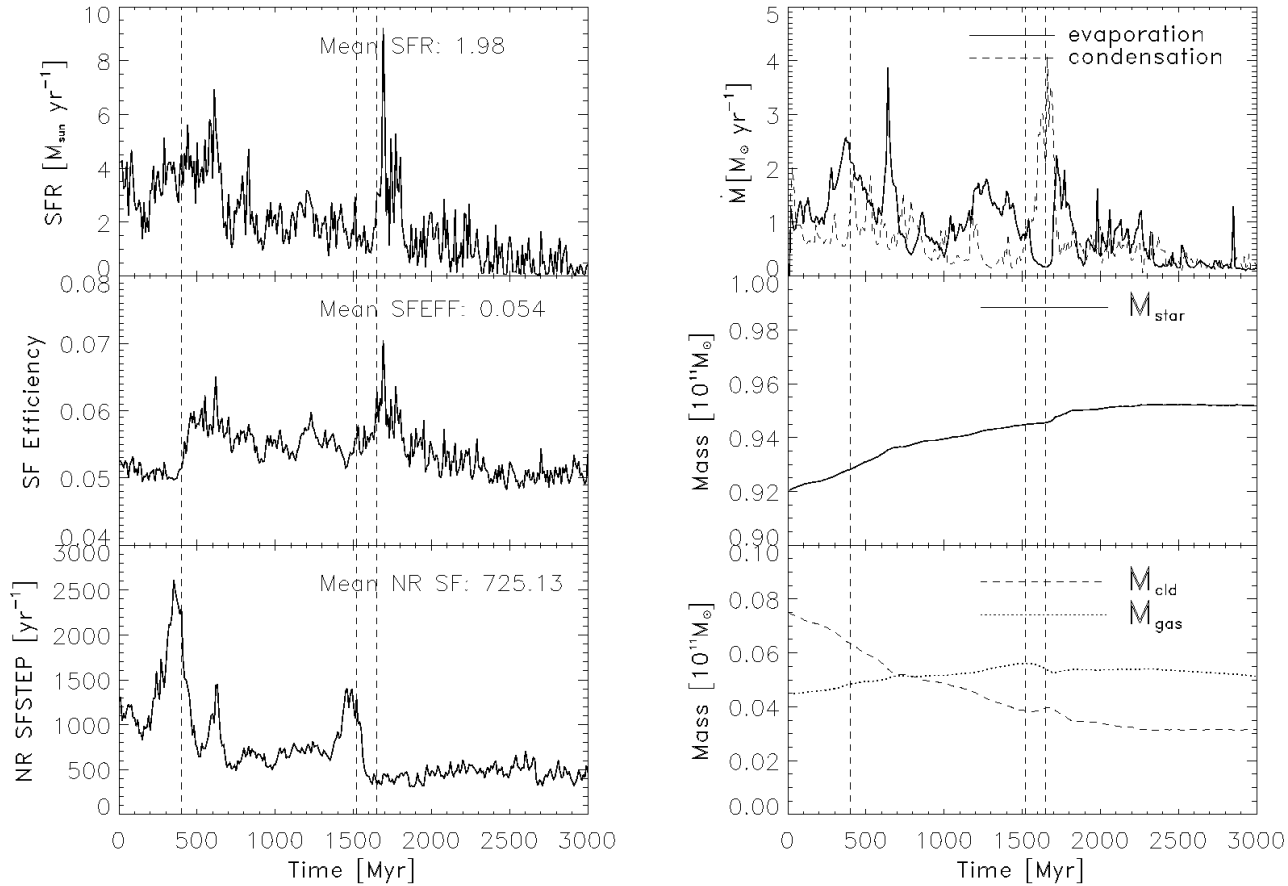


Fig. 4 Evolution of star formation (left) and mass (right): the star formation rate (left, top), the evolution of the mean star formation efficiency (left, middle), and the number of star formation processes within a sampling period of 10 Myr (left, bottom). On the right side, the evolution of the evaporation and condensation rates (top), the evolution of mass of stars (middle), and the evolution of mass of the ISM (bottom) are plotted. The three vertical dashed lines indicate the first passage, the second passage, and the beginning of the merging.

outweighs condensation. As a result only 3% of baryonic matter are molecular clouds in the end of the simulation. In comparison, the fraction of molecular clouds was initially 8%.

- Due to star formation and related feedback during the first passage the stellar mass as well as the mass of the diffuse ISM rises more steeply.
- As a consequence of the merging accompanied by enhanced star formation, the stellar mass increases rapidly. In Fig. 4 one can also distinguish a short period of time, within which the diffuse ISM is diminished by condensation, whereas the cloud mass increases.

Fig. 7 shows a snapshot of the interaction at $t = 550$ Myr - 150 Myr after the first passage. Different components are plotted separately in order to emphasise the multi-phase properties of our simulation. In the uppermost panel a surface density map of stars is shown. It is easy to pinpoint the two galaxies, a bridge connecting them, and tails protruding from each of them. The cold molecular clouds (second panel from top) follow the distribution of the stars very well. However, the tail of the warm phase is considerably shorter as one can deduce from the third and forth panel which show

a density map of the diffuse ISM and a temperature map, respectively. In the temperature map it is easy to identify two phases: a warm phase in the galactic disks, the bridge, and the tails, and a hot phase primarily located in the halo, but also in hot supernovae bubbles. The reason behind the shortened tails is the initial setup of the diffuse gas component. Due to the initial collapse, the warm gaseous disk is initially much smaller than the stellar disk and grows only slowly in size. At the beginning of the interaction the warm gaseous disk is still smaller than the stellar disk. Since the utmost part of the tail evolves from the utmost part of the disk, the tail of the warm ISM is not as extended as the stellar tail or the tail of the cold phase.

5 Conclusions & Outlook

We have presented a study of an equal size major merger by means of a multi-phase ISM code described in Harfst et al. (2006). We have focused on the evolution of the star formation rate as well as on the evaporation and condensation rates. The multi-phase nature of the code allows for an extensive analysis of mass transfer involving galaxy interac-

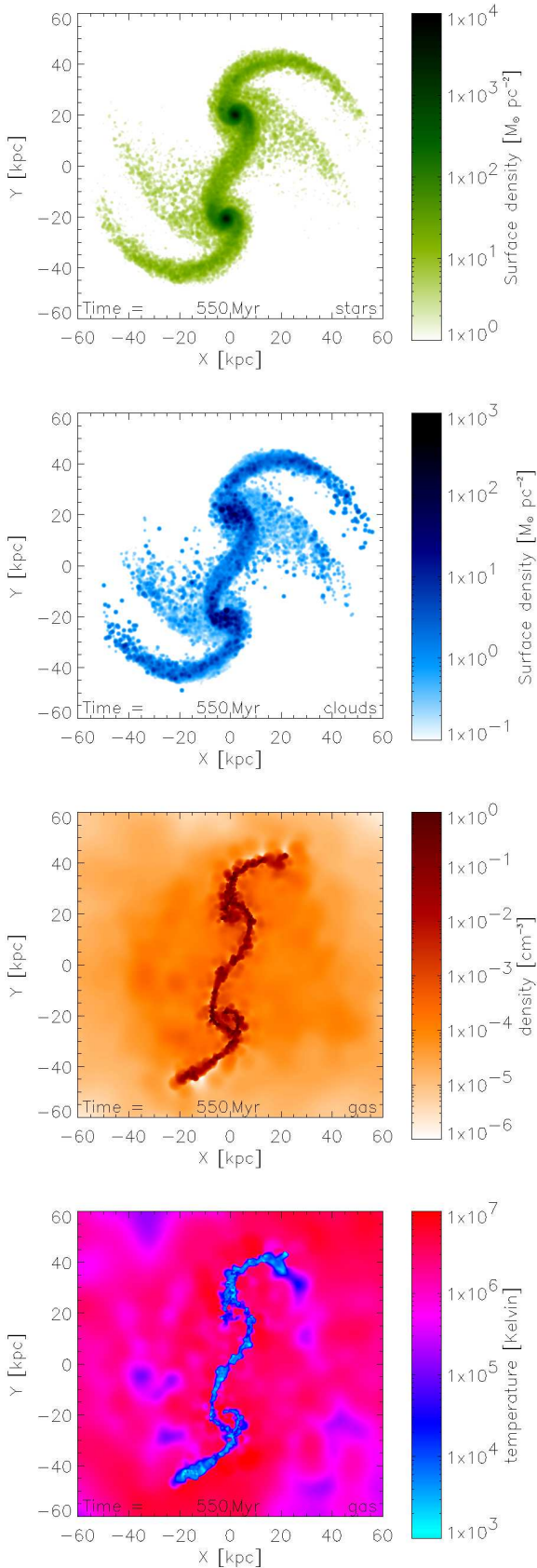


Fig. 7 This figure shows from top to bottom a surface density map of stars, a surface density map of clouds, a density map of the diffuse ISM, and a temperature map of the diffuse ISM at time $t = 550$ Myr (i.e. 150 Myr after the first passage).

tions. Furthermore, the star formation prescription according to Elmegreen & Efremov (1997) allows to follow the star formation efficiency during the interaction locally. The star formation rate as well as the star formation efficiency increases due to the first encounter and the merging of the nuclei. In the mean the star formation efficiency is only 5%, but at some locations, usually in the centre of the galaxies, but also in the bridge or the tails, the star formation efficiency can be much higher - up to 55%. Yet, a drawback of our models is an initial gaseous disk which is smaller than the stellar disk resulting in a lack of SPH particles at the tip of the tails. Therefore, an improved setup of the SPH component is needed in order to study substructures, such as tidal dwarf galaxies, within the tip of the tails.

Acknowledgements. JW is a member of the Initiativkolleg (IK) 'The Cosmic Matter Circuit' I033-N of the University of Vienna. The numerical simulations were performed on the Grape cluster of the Institute of Astronomy of the University of Vienna. CT is grateful for financial support by the project TH511/9-1 within the DFG Priority Programme 1177 'Galaxy Evolution'. SH is supported by the NWO Computational Science STARE project 643200503.

References

- Arp, H.: 1966, Atlas of peculiar galaxies, California Institute of Technology, Pasadena
- Barnes, J. E.: 1988, ApJ 331, 699
- Barnes, J. E., Hernquist, L.: 1992, ARA&A 30, 705
- Bournaud, F., Duc, P.-A.: 2006, A&A 456, 481
- Cox, T. J., Primack, J., Jonsson, P., Somerville, R. S.: 2004, ApJ 607, L87
- Dehnen, W.: 2002, JCoPh 179, 27
- di Matteo P., Bournaud F., Martig M., Combes F., Melchior A.-L., Semelin, B.: 2008, A&A 492, 31
- Duc, P.-A., Bournaud, F., Masset, F.: 2004, A&A 427, 803
- Elmegreen, B. G., Efremov, Y. N.: 1997, ApJ 480, 235
- Harfst, S., Theis, C., Hensler, G.: 2006, A&A 449, 509
- Hernquist, L., Katz, N.: 1989, ApJS 70, 419
- Holmberg, E.: 1941, ApJ 94, 385
- Karl, S. J., Naab, T., Johansson, P. H., Theis, C., Boily, C. M.: 2008, Astronomische Nachrichten 329, 1042
- Kennicutt, Jr. R. C.: 1998, ApJ 498, 541
- Kuijken, K., Dubinski, J.: 1995, MNRAS 277, 1341
- Lada, C. J., Lada, E. A.: 2003, ARA&A 41, 57
- McKee, C. F., Ostriker, J. P.: 1977, ApJ 218, 148
- Mihos, J. C., Hernquist, L.: 1996, ApJ 464, 641
- Pfleiderer, J., Siedentopf H.: 1961, Zeitschrift für Astrophysik 51, 201
- Schmidt, M.: 1959, ApJ 129, 243
- Semelin, B., Combes, F.: 2002, A&A 388, 826
- Springel, V., Hernquist, L.: 2005, ApJ 622, L9
- Theis, C., Hensler, G.: 1993, A&A 280, 85
- Toomre, A., Toomre, J.: 1972, ApJ 178, 623
- Wetzstein, M., Naab, T., Burkert, A.: 2007, MNRAS 375, 805